



Research Note

Potential of Solar UV Radiation for Inactivation of Coronaviridae Family Estimated from Satellite Data

Fernanda R.S. Carvalho¹, Diamantino V. Henriques¹ , Osvaldo Correia^{2,3,4} and Alois W. Schmalwieser^{5*} 

¹Portuguese Institute for Sea and Atmosphere, Ponta Delgada, Portugal

²Centro de Dermatologia Epidermis, Instituto CUF, Porto, Portugal

³Portuguese Skin Cancer Association, Porto, Portugal

⁴Center for Health Technology and Services Research (CINTESIS), Basic and Clinical Immunology Unit, Department of Pathology, Faculty of Medicine, University of Porto, Porto, Portugal

⁵Institute of Physiology and Biophysics, University of Veterinary Medicine, Vienna, Austria

Received 4 June 2020, revised 12 October 2020, accepted 15 October 2020, DOI: 10.1111/php.13345

ABSTRACT

The pandemic COVID-19 disease affects people dramatically overall the globe by illness and death. Several strategies are applied to restrict the spread of this disease such as lockdown, adequate social distance in different activities, hand disinfection and the use of masks. Potential hazard outdoors comes from released viruses, which may remain in the air for a while and settle down afterward and contaminating surfaces. Solar ultraviolet radiation (UVR) is known to act as a natural environmental virucide. The virucidal effectivity of UVR depends on a first order on the sensitivity of the virus against UVR as well as on the amount of incoming UVR. Here, we present estimates of the potential of solar UVR in inactivating SARS-CoV-2 in the environment. This is done by combining DNA-damaging surface solar UVR retrieved by satellites and the available information on fluence for inactivation of *Coronaviridae*. Our results show that solar UVR has a high potential to inactivate these viruses, but the degree depends strongly on location and season. In the subtropics (Sao Paulo, 23.5°S), the daily survival fraction is lower than 10^{-4} during the whole year, while close at norther latitudes (Reykjavik, 64°N), such a reduction can be found in June and July only.

INTRODUCTION

From late December 2019 until the edition of this note, WHO reported globally 6 057 853 COVID-19 cases and 371 166 deaths (1). COVID-19 disease is caused by a new kind of coronavirus (*Coronaviridae*), named SARS-CoV-2, and was declared a pandemic on 11 March 2020 (2), just three months and 11 days after the first reported outbreak in Wuhan City, Hubei

Province of China. Within a few weeks, COVID-19 had spread over mid and high latitudes (30°–65°) of the Northern Hemisphere from east to west, suggesting that cold and dry weather could have a role in the spread of the disease (3). Despite the sampling representativeness of the reported COVID-19 cases, a global scale pattern can suggest that weather conditions might have a role in the spread of the outbreak. Although humidity, air temperature and other variables can affect virus survival, solar ultraviolet radiation is the primary virucidal agent in the environment (4,5,6,7). It is well known that solar ultraviolet (UV) radiation acts as a natural environmental virucide, because it causes—among others—photodimer formation between the pyrimidine bases in DNA and RNA, resulting in conformational changes that interrupt the viral replication process (8,9).

To determine solar inactivation of viruses, it is necessary to estimate the sensitivity of viruses over the whole UV range (100–400 nm). Most of the information published on UV inactivation of viruses has been based on exposure to radiation from a low-pressure mercury vapor (germicidal) lamp, with the primary emission at 254 nm (10). However, solar irradiance of 254 nm does not reach the earth's surface. To overcome this difficulty, extrapolation from 254 nm will be required for most viruses by using the known spectral responses (8,10,11) of others. The sensitivity of a virus to UV radiation is determined via a survival curve, with the logarithmic surviving fraction as a function of UV exposure D or fluence. A frequently used measure for inactivation is the fluence D_{90} , the effective radiant flux necessary to inactivate 90% (or 10% survival fraction) of the viruses. Based on the ssRNA genomic model, Sagripanti and Lytle (11) found a D_{90} value for SARS-CoV-2 of 6.9 J m^{-2} in aerosols that is consistent with the value found by Weiss (12) for coronavirus. Walker (13) found D_{90} being 6.6 J m^{-2} for coronavirus in air. Sensitivity of airborne viruses to UV radiation is higher than in liquid suspensions. However, the exact ratios can vary considerably between microbial species (14). For comparison, D_{90} for influenza A virus is higher than for coronavirus: 19 J m^{-2} in air and 20 J m^{-2} in water (14), needing a much longer exposure time to reach the same inactivation level with the same photon energy. Recent experiments using simulated UV sunlight at

*Corresponding author email: alois.schmalwieser@vetmeduni.ac.at (Alois W. Schmalwieser)

© 2020 The Authors. Photochemistry and Photobiology published by Wiley Periodicals LLC on behalf of American Society for Photobiology

This is an open access article under the terms of the Creative Commons Attribution-NonCommercial-NoDerivs License, which permits use and distribution in any medium, provided the original work is properly cited, the use is non-commercial and no modifications or adaptations are made.

20 °C and different relative humidity conditions show that radiant fluxes equivalent to summer solstice at 40° latitude can inactivate 90% of SARS-CoV-2 in 8 min on aerosol-simulated saliva (15) and in 6.8 min on surfaces (16). Using the same TUV model (17) and the same default atmospheric conditions, it was possible to estimate the correspondent inactivation fluences (D_{90}) as 2.1 and 1.8 J m⁻², respectively.

In this paper, we have combined the knowledge of coronavirus inactivation with available UV radiation data from satellites to estimate exposure times for inactivation and survival ratios for this virus family and with that the potential influence of solar UV radiation.

MATERIALS AND METHODS

Measurements of biologically effective UV radiation from satellites are available as spectrally weighted (e.g. with the action spectrum of DNA damage) values of daily radiant exposure (horizontal flat surface). In this section, we will show how the weighted radiant exposure can be converted into virucidal acting fluence (spherical surface) and how it can be calibrated in respect to the fluence and response for coronavirus. From these, practical measures such as the daily survival fraction of viruses and the duration for a certain degree of inactivation are derived to demonstrate the potential influence of solar UV radiation.

Satellite data. UV radiation data were obtained from the TEMIS (Tropospheric Emission Monitoring Internet Service). TEMIS provides a variety of UV radiation products, which are produced by assimilation of data from several instruments (GOME, GOME-2, SCIAMACHY and OMI) aboard polar orbiting satellites. Data from TEMIS have been widely used for the estimation of surface UV radiation (e.g. 18,19) and for some medical applications (e.g. 20,21). One of the products available from the TEMIS is the DNA-damaging daily radiant exposure H_{DNA} (22):

$$H_{DNA} = \int_{t=\text{sunrise}}^{t=\text{sunset}} \int_{\lambda=100\text{nm}}^{\lambda=400\text{nm}} E(\lambda, t) S_{DNA}(\lambda) d\lambda dt \quad (1)$$

where E is the clear-sky surface downward spectral irradiance for a given wavelength λ and time t , and S_{DNA} is the spectral effectivity (action spectrum) for DNA damage in the UV range.

This quantity is estimated for each point of a regular grid (0.25° × 0.25°) at the earth's surface, considering the altitude and atmospheric parameters such as total ozone column and aerosol optical depth. Cloud modification factors (CMF) are used from MSG (Meteosat Second Generation) geostationary satellites data to correct clear-sky irradiance for cloudiness.

Radiant exposure and Fluence. Irradiance E , the radiant flux received by a plane surface, is not the most relevant radiative quantity to airborne particles (6). Geometry of an airborne particle is rather spherical, and its orientation in respect to the sun is rather random. The radiation received by a particle's surface from all directions is also called fluence rate and therefore is different from the irradiance referred above (23). The same holds for their time integrals: radiant exposure H and fluence Φ . Madronich (6) found that the fluence rate (respectively fluence) is systematically larger than the irradiance (respectively radiant exposure) by a certain factor R :

$$\Phi = H \cdot R \quad (2)$$

The factor R is around 2 or higher near the surface, and this factor increases with altitude. Madronich (6) proposed the following parametrization for the ratio R :

$$R \approx 2.6 + 0.8z - (0.8 + 0.5z)\cos\Theta_N \quad (3)$$

where z is the local altitude in km and Θ_N the solar zenith angle at noon. It should be noted that this parameterization is based on DNA-damaging radiation, 24 h average and clear-sky conditions (6).

Action spectra of DNA and RNA damage and scaling. The DNA damage action spectrum provided by Setlow (24) is generally used for the computation of the H_{DNA} . Laboratory experiments have shown that the rates of RNA damage closely mirror the loss of viral infectivity, which demonstrates that genomic damage is the dominant cause of inactivation (10). Lytle and Sagripanti (8) showed that there is little or no difference between the action spectra for the inactivation of DNA and RNA viruses. With that, the DNA damage action spectrum $S_{DNA}(\lambda)$ can be used as a proxy for the RNA inactivation action spectrum $S_{RNA}(\lambda)$ (6):

$$S_{RNA}(\lambda) = S_{DNA}(\lambda) \quad (4)$$

The action spectrum used by TEMIS (based on Setlow) is normalized at 300 nm. The inactivation fluence (D_{90}) is given for 254 nm, and therefore, a linear scaling (calibration) is necessary to bring the TEMIS data in agreement with the D_{90} value. The scaling factor f corresponds to the ratio of the sensitivity at 254 nm ($S_{DNA}(254 \text{ nm})$) and the sensitivity at 300 nm ($S_{DNA}(300 \text{ nm})$):

$$f = \frac{S_{DNA}(254 \text{ nm})}{S_{DNA}(300 \text{ nm})} \quad (5)$$

Daily fluences, exposure times and inactivation fractions. The daily fluence for RNA damage Φ_{RNA} can be computed straightforward by using H_{DNA} ($=H_{RNA}$) from TEMIS for each day and place:

$$\Phi_{RNA} = \frac{H_{RNA}}{f} \cdot R \quad (6)$$

From daily fluence values, practical measures such as the daily survival fraction S or the time necessary to inactivate a certain percentage of viruses $T_{\%}$ can be estimated.

Given the large uncertainty of the available data for SARS-CoV-2 UV radiation sensitivity, this work will use the lowest and the highest D_{90} values found in the peer-reviewed literature as references for the most and least prudent scenarios, respectively. From these, the lowest D_{90} is 1.8 J m⁻² (15) and the highest is 7 J m⁻² (11).

A survival fraction of 10% (D_{90}) is maybe too high for reducing the risk of infection significantly. Therefore, it may be useful to estimate the fluence for 99% virus inactivation (1% survival) or for even lower levels of survival (11). In this way, sterilization level (10⁻⁶ survival) fluences (D_S) will be used. The lowest D_S is calculated to be 10.8 J m⁻² and the highest to be 42.0 J m⁻².

As shown by laboratory experiments with viruses in culture medium, the material in aerosols (as created by COVID 19 patients and carriers) may shield the virus from UV radiation (16). With that, the virus survival fraction becomes higher; respectively, a higher fluence is necessary to gain a certain level of reduction. Altogether, the required fluence for sterilization, when viruses are shielded, becomes 20 times larger than for a 10% reduction (11). Applying this, our lowest and highest sterilization fluences (D_S) become 36 and 140 J m⁻², respectively.

The exposure time T_S necessary for virus sterilization can be computed for a given day and place dividing the D_S values by the respective computed daily average fluence rate:

$$T_S = \frac{\Delta T \times D_S}{\Phi_{RNA}} \quad (7)$$

where ΔT is the length of the day (from sunrise to sunset). In practice, T_S corresponds to the average fluence rate which occurs at the 1st and 3rd quarters of the (cloudless) day (e.g. 9:00 and 15:00 when daylight lasts 12 h from 6:00 to 18:00). At noon, this time is just half and is longer before and after.

Exposure times for several inactivation levels are given in Table 1 for the highest and lowest sensitivities for different fluence rates F_{RNA} and values of daily fluence (for 12 h daylight), respectively. It can be seen that exposure times required for the same inactivation level as well as the daily fluence can vary significantly due to the uncertainties found for SARS-CoV-2 UV sensitivity. In addition, for the same fluence level, exposure times range from several minutes to several hours.

The second practical measure, the daily survival fraction S , can be calculated by using the definition expression:

Table 1. Exposure time ranges (lowest to highest sensitivity) for several inactivation levels in dependence of mean fluence rate, respectively, corresponding daily fluence value (see Eq. 5) for SARS-CoV-2.

| F_{RNA} (mW m ⁻²) | Φ_{RNA} (J m ⁻²) | Inactivation level | | | |
|---|---|--------------------|---------|---------|---------------|
| | | 90% | 99% | 99.9% | Sterilization |
| 4.63 | 200 | 6'–25' | 26'–2 h | 52'–3 h | 2–8 h |
| 2.32 | 100 | 13'–50' | 52'–3 h | 2–7 h | 4–17 h |
| 1.16 | 50 | 26'–2 h | 2–7 h | 3–13 h | 9–34 h |

$$S = \frac{N}{N_0} \equiv e^{-k\Phi_{\text{RNA}}} \quad (8)$$

where N and N_0 are the numbers of active viruses after and before the exposure to the daily fluence Φ_{RNA} . The factor k is gained by converting Eq. 8 and applying the known D_S value (for fluence and the corresponding survival fraction for 10^{-6} ($S = N/N_0 = 10^{-6}$)):

$$k = \frac{-\ln(10^{-6})}{D_S} \text{ or } k = \frac{-\lg(10^{-6})}{D_S \cdot \lg(e)}$$

To sum up, the above satellite data and methods will be used to estimate time series of daily fluences, exposure times for sterilization and survival ratios of coronavirus family at selected locations and for daily global maps. Constants used in the computations of exposure times and survival fractions for sterilization level are given in Table 2.

RESULTS

Time series for some selected locations

Four different locations have been selected to illustrate the influence of seasons at different climates and latitudes on the inactivating potential of solar UV radiation. The selected sites are Sao Paulo (23.625°S, 46.625°W, 779 m a.s.l.), Lisbon (38.875°N, 9.125°W, 132 m a.s.l.), Vienna (48.125°N, 16.375°E, 201 m a.s.l.) and Reykjavik (64.125°N, 21.875°E, 55 m a.s.l.). For each selected location, the cloud-modified DNA-damaging UV radiant exposure H_{DNA} in kJ m⁻² is taken from the closest center of a grid cell (0.25°×0.25°) for each day from 22 January 2005 to 19 April 2020. From each H_{DNA} time series, daily T_S and daily survival fractions S were computed using the described methods. Figure 1 shows the daily cloud-modified fluence for RNA damage Φ_{RNA} for each site. It can be seen that fluence shows a clear annual cycle at all locations with values close to zero in winter. The maximum values differ by a factor of around 4 between Sao Paulo and Reykjavik. In addition, the shape of the annual course differs between locations. At Reykjavik, the period with very

Table 2. Constants used for T_S and S calculations.

| Constant name | Value |
|---------------|---|
| f | 29.8247 |
| D_S (low) | 36 J m ⁻² |
| D_S (high) | 140 J m ⁻² |
| k (low) | 0.383764 m ² J ⁻¹ |
| k (high) | 0.098682 m ² J ⁻¹ |
| ΔT | 12 h |

low fluences is long (September to March), while at Sao Paulo, this period is restricted to a few days per year (June).

Figure 2 shows the times series of T_S for coronavirus between low and high D_S and for the four selected sites.

Figure 3 shows the estimated $T_{S\text{-low}}$ (left scale), respectively, $T_{90\text{-low}}$ (right scale) at the selected sites (using the lowest D_S for calculation). It becomes evident that there are obvious differences between the four locations. At Sao Paulo, $T_{S\text{-low}}$ is below 6 h during almost the whole year and $T_{S\text{-low}}$ is longer than available daylight hours on just a few days in June. At Lisbon, $T_{S\text{-low}}$ is shorter than 6 h between April and October, and at Vienna, between May and August. At Reykjavik, $T_{S\text{-low}}$ is longer than 6 h during the whole year. However, there are many days between the equinoxes that last long enough to reach $T_{S\text{-low}}$, because the duration of daylight reaches 24 h in summer. Looking on the $T_{90\text{-low}}$ (right scale), there are many days on which $T_{90\text{-low}}$ is below 1 h at all locations.

Survival ratio for high and low D_S after a daily exposure is shown in Figure 4 for the same locations.

Figure 5 shows the estimated daily survival fraction for coronavirus after daily solar exposure estimated for Sao Paulo, Lisbon, Vienna and Reykjavik for 2019. It can be seen that at all four locations, there are periods during which the daily fluence is high enough to inactivate 99.99% (10^{-4} survival fraction) of the viruses. At Sao Paulo, this period lasts over the whole year (except for one single day). At Lisbon, this period lasts from March to the end of October, at Vienna, this period lasts from May to October, and at Reykjavik, this period lasts from May to August.

The potential of solar UV for inactivation is zero in Vienna only on selected days with snowfall, but at Reykjavik, it is zero from October to the end of February. At Lisbon, the sun is effective for inactivation during the whole year. There are only a few days in December on which inactivation is less than 90%.

Daily maps for the Central Hemisphere

TEMIS provides daily maps of H_{DNA} for clear sky on a global scale, but only cloud-modified H_{DNA} grids (in HDF4 format, based on MSG cloud data) for the hemisphere centered at (0°N, 0°W). Daily fluences, exposure times and survival fractions were computed for each grid point using the already mentioned methods for Northern Hemisphere winter and spring days (21 December 2019 and 14 April 2020). The resulting maps are shown in Figs. 6–8

21 December 2019 was selected as an example of pre-pandemic conditions and because it is close to the winter solstice (of the Northern Hemisphere), when solar radiation at the surface reaches the annual minimum. By the start of this work (around 14 April 2020), most countries in Europe had already reached the first peak of new daily reported cases of this pandemic (32). 14 April 2020 was therefore selected as an example for conditions after the peak and as an example of a spring day (not that far from the equinox).

Figure 6 depicts the latitudinal variation of daily virucidal fluence at the surface on a winter/summer (Fig. 6a) and a spring (Fig. 6b) day. The highest values can be found in the continental regions of the tropics and of the Southern Hemisphere (summer). The lowest values occur in the Northern Hemisphere (winter). Therefore, the spatial amplitude of fluence is larger at the solstices than at the equinoxes. The effect of the topography is also visible, by the highest daily fluence in the Andes (>800 J m⁻²)

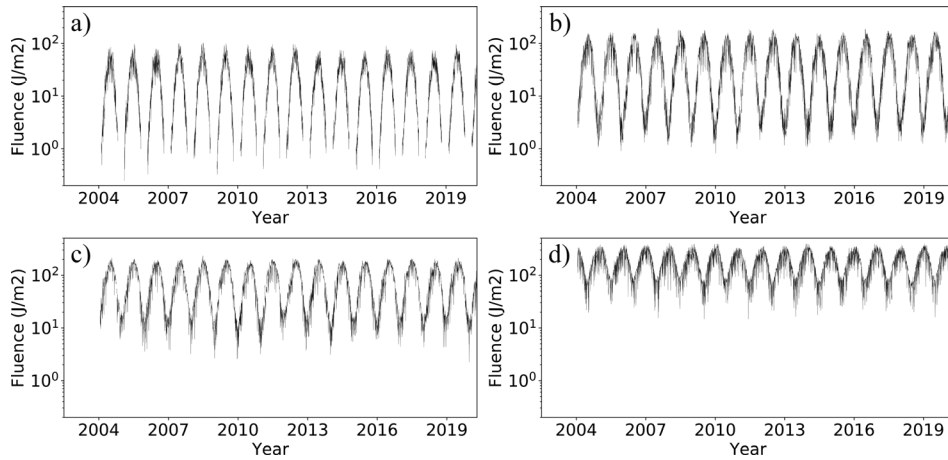


Figure 1. Time series of daily fluences for RNA damage estimated for (a) Reykjavik, (b) Vienna, (c) Lisbon and (d) Sao Paulo.

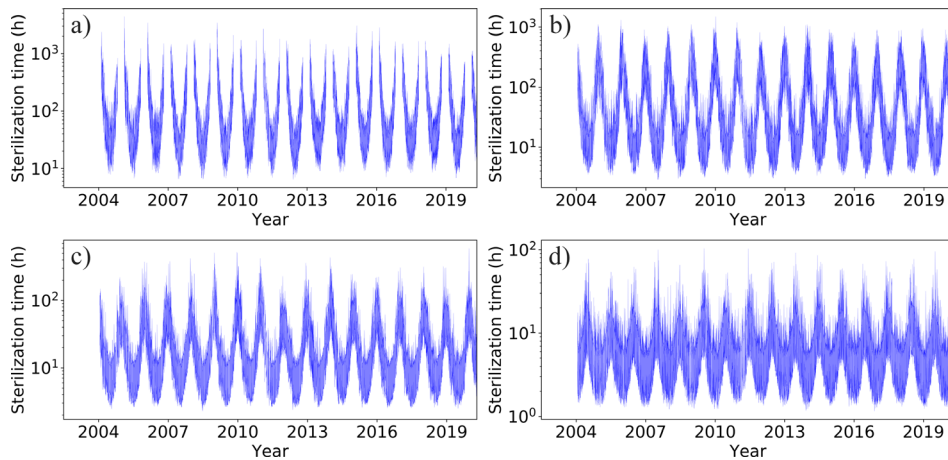


Figure 2. Time series of daily exposure time ranges (hours) between high and low D_s for SARS-CoV-2 sterilization estimated for (a) Reykjavik, (b) Vienna, (c) Lisbon and (d) Sao Paulo. [Color figure can be viewed at [wileyonlinelibrary.com](#)]

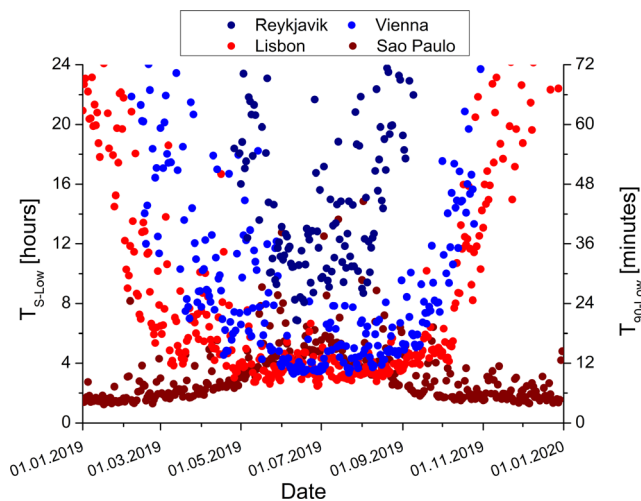


Figure 3. Daily exposure times for sterilization of coronavirus, estimated at four selected sites for 2019. The scale on the right indicates exposure times for 90% inactivation.

(both figures). These figures show also the effect of cloudiness patterns (associated with synoptic systems, which naturally reduce UV radiation reaching the surface (dark blue and black patterns in both figures)).

The maps in Fig. 7 show a remarkable zonal variation of sterilization times, by increasing from the tropics to the poles. The lowest values occur in the continental regions of the tropics, where virucidal fluence is highest. The shortest times can be found in the Andes region and are shorter than one hour. The role of cloudiness in influencing sterilization times is even more important. The map in Fig. 7b shows that sterilization times can vary from 2 to 10 h in within a few kilometers (horizontally). Our results show that sterilization times across Europe near the winter solstice of 2019 (Fig. 7a), that is, before the pandemic, are longer than 24 h. Contrary, these times were generally between 8 and 12 h in spring (Fig. 7b).

Most of the Northern Hemisphere above 30°N receives less than 120 J m⁻² per day near the winter solstice (Fig. 7), leading to sterilization times longer than 3 h to several days over most of Europe (Fig. 8). Corresponding daily survival fractions are generally greater than 10⁻⁶ for Europe and well below sterilization levels (<10⁻⁶) at tropical latitudes and southern latitudes

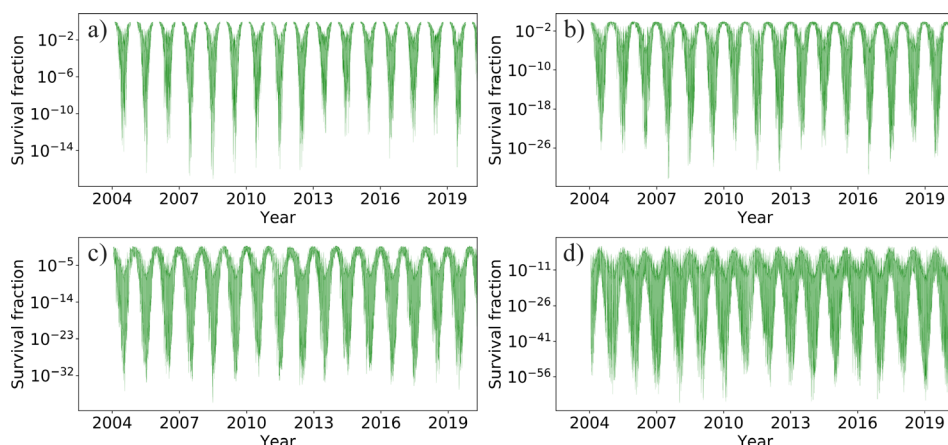


Figure 4. Time series of daily survival fraction ranges between high and low D_s of SARS-CoV-2 after a daily solar exposure estimated for (a) Reykjavik, (b) Vienna, (c) Lisbon and (d) Sao Paulo. [Color figure can be viewed at wileyonlinelibrary.com]

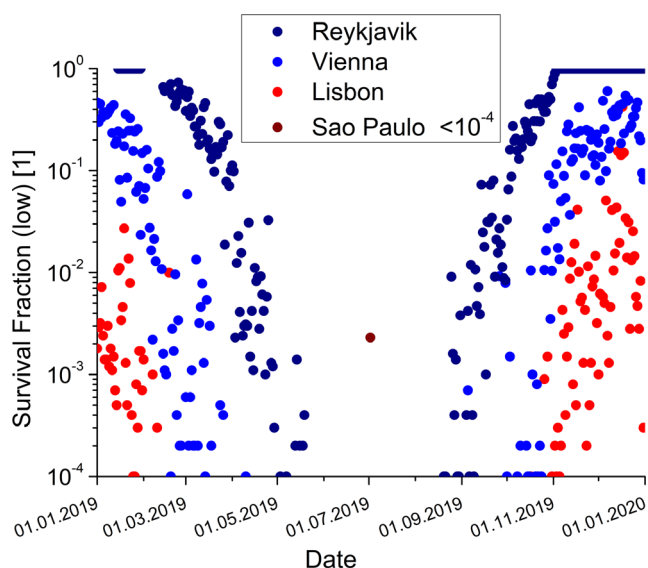


Figure 5. Daily survival fraction of coronavirus after daily solar exposure estimated for Reykjavik, Vienna, Lisbon and Sao Paulo ($< 10^4$ during almost the whole year) for 2019.

below 30°S. These results suggest that UV exposure over a whole day at the winter solstice (Fig. 8a) may not be enough for outdoor virus sterilizing for almost the entire European continent. On the other hand, these figures show that the daily fluence can be high enough in spring to reach sterilization levels in large parts of Europe. At lower latitudes ($< \pm 30^\circ$), daily fluence is generally higher than 300 J m^{-2} all the year. Therefore, T_S is in the range of 2 or 6 h, and therefore, daily survival fractions are clearly below the sterilization threshold (Fig. 8). These results also suggest that daily sunlight exposure in spring can be enough to sterilize most of the outdoor Coronavirus in almost the entire Europe, while at lower latitudes, it is sterilized almost all the year.

DISCUSSION

There is some evidence that meteorological parameters and UV radiation correlate with the spread of viral diseases such as influenza (24-26). Recent studies concluded that high air temperature, humidity and UV solar radiation have a decline effect on COVID-19 transmission rate (4,27,28,29). Aerosol particles can carry active viruses and remain for several hours in the air before

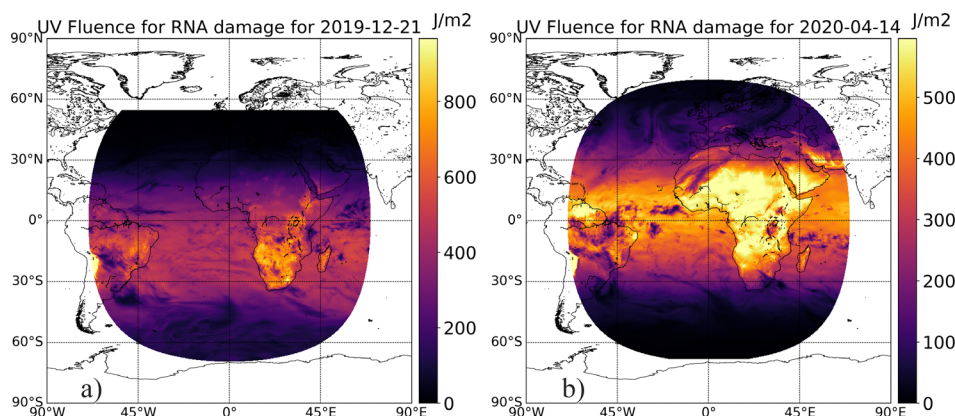


Figure 6. Daily cloud-modified fluence (J m^{-2}) for RNA damage estimated for (a) 21 December 2019 and (b) 14 April 2020.

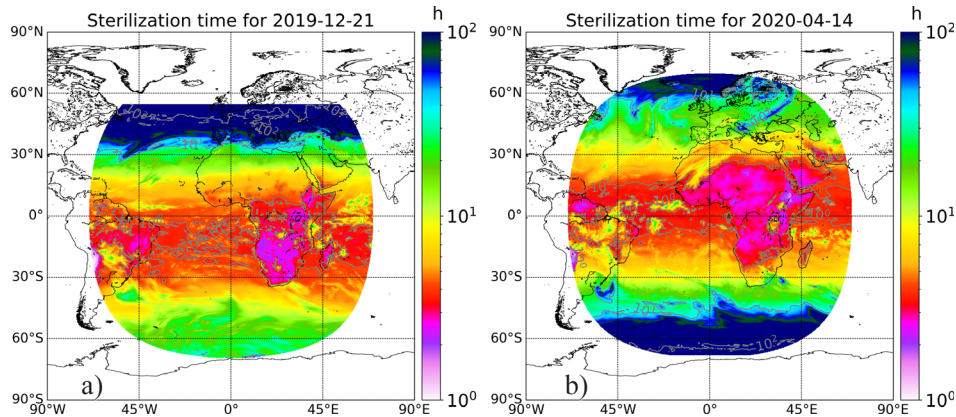


Figure 7. Daily exposure times (hour) for SARS-CoV-2 sterilization estimated for (a) 21 December 2019 and (b) 14 April 2020. Dashed colored areas correspond to high D_s and solid gray lines to low D_s .

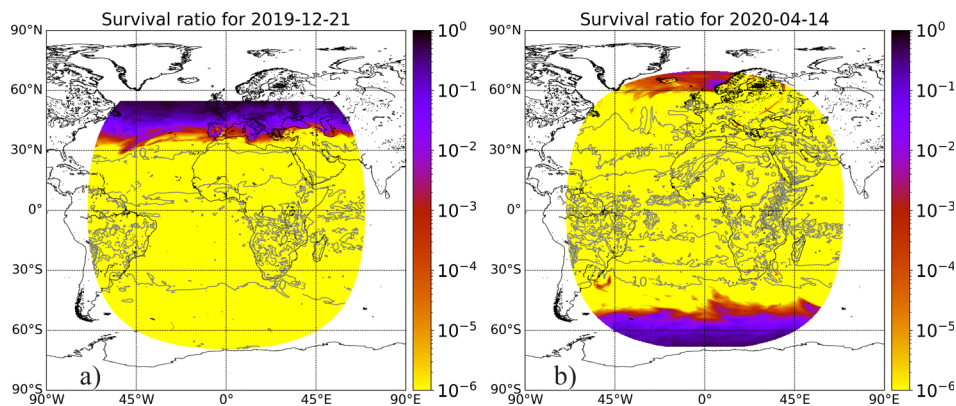


Figure 8. Daily survival fraction for SARS-CoV-2 after a daily exposure estimated for (a) 21 December 2019 and (b) 14 April 2020. Dashed colored areas correspond to low D_s and solid gray lines to high D_s .

settling down on surfaces (30). Several laboratory studies have estimated the survival times of SARS-CoV-2 for several types of surfaces and environmental conditions (16,30,31), ranging from 24 h (paper) to 9 days (plastic) without UV irradiation. However, UV radiation is a high effective virucide agent and solar UV is the most important natural virucide. Its virucidal potential depends on the amount of the effective radiant exposure or fluence that reaches the surfaces or the airborne particles that contain the active viruses.

In this paper, we have estimated the potential of solar UV radiation to inactivate Coronaviridae and with that to the spread of COVID-19. We have used available information on inactivation together with globally available satellite UV radiation data. As shown by these, the RNA-damaging daily fluence can vary from 0 to several hundreds of J m^{-2} along the year and from high to low latitudes. Additionally, we calculated the corresponding survival fraction and T_S as a practical measure.

The exponential dependence of the survival fraction on the fluence leads to variations on survival fractions and exposure times of several orders of magnitude between different latitudes and different seasons. The disinfection power of solar UV radiation can be compared with other biocidal agents. For instance, cleaning for 30 s with 5% ethanol solution is equivalent to 200 J m^{-2} of sunlight irradiation (31).

Some assumptions must have been made for this work, which may lead to some uncertainties in the gained results:

- Surface UV irradiance data are remote sense retrievals from satellite measurements and therefore have lower accuracy than ground-based measurements.
- Most of the day-to-day variability as well as some spatial variability in surface UV radiant exposure is due to the presence of clouds. Cloud effects on UV surface irradiance are corrected using MSG geostationary satellite data, adding additional uncertainty to the H_{DNA} data used.
- There is no specific action spectrum for SARS-CoV-2 inactivation, but DNA and RNA damage action spectra are close.
- The parameterized conversion of daily radiant exposure into fluence used in this work was validated for clear-sky conditions only and therefore can be another source of uncertainty for cloudy days.
- Few peer-reviewed works on UV sensitivity of SARS-CoV-2 were found, and published D_{90} values may possess uncertainties. While relative uncertainties in fluence cause the same uncertainties in exposure times, small uncertainties in fluences lead to very large uncertainties in daily survival fractions.

It should be noted that our results are intended for longer periods like weeks and months and not for a daily basis. Our results are applicable to identify seasonal trends or special periods.

Our results suggest that solar UV exposure in spring (fall) and summer can be the main natural limiting factor for the virus survival outdoors, because more than 90% of the viruses can be inactivated in less time than other natural environmental factors (e.g. surface type, air temperature and humidity) can do. The estimated T_{90} and T_S show that UV radiation may have minor effects on the direct viral transfer from person to person in air, because this can occur within minutes. However, our estimates show that viruses remaining in the air or adhering at surfaces are clearly affected by solar UV radiation. Even in Iceland, the solar UV is able to inactivate 90% within 30–100 min in summer and sterilization within a day. At Sao Paulo, this ability lasts the whole year.

Geographic latitude and atmospheric ozone can limit the maximum values of UV radiation and therefore of virucidal fluence at the surface. However, other factors such as topography and cloudiness also play a very important role in the distribution of UV radiation at the surface and consequently in the inactivation times as well as in the survival fraction. Our results suggest that in December (2019), daily solar irradiation would not be sufficient to reach a level of sterilization across the European continent (Fig. 8a). This may have enabled survival conditions outdoors for coronavirus enough to stay infective during several hours or even over whole days (Fig. 7a). In mid-April 2020, after the first peak of the pandemic in Europe (32), the survival fractions over the European continent were equivalent to or even below the sterilization levels (Fig. 8b). This suggests that infections contracted outdoors may have been inhibited in some way by sterilizing the coronavirus by solar UV radiation.

It should be mentioned that among the shades, the survival fractions are higher. It should be also mentioned that glass windows block most of the solar UV-B radiation (280nm–315nm) and therefore inhibits the virucidal effectiveness of sunlight.

Knowledge of environmental conditions, humidity, temperature and UV radiation can be important for neutralizing or minimizing the contagiousness of contaminated surfaces or even for mitigating the aggressiveness of the virus contagiousness. Progressive deflation is essential for the economic recovery and normalization of all recreational, educational and occupational activities. For this, all individual and community protection measures are important at this stage and during a possible second wave to minimize the risk of contagiousness. We hope that these data can be a contribution to complementary studies on the role of solar UV radiation in reducing the contagiousness of contaminated surfaces and can act as an additional tool for individual and collective protection.

REFERENCES

1. WHO (2020) *Coronavirus Disease*, World Health Organ., Geneva. Situation report No. 133 (June 1st).
2. WHO (2020) *Coronavirus Disease*, World Health Organ., Geneva. Situation report No. 109 (May 8th).
3. Sajadi, M. M., P. Habibzadeh, A. Vintzileos, S. Shokouhi, F. Miralles-Wilhelm and A. Amoroso (2020) Temperature, humidity, and latitude analysis to estimate potential spread and seasonality of coronavirus disease 2019 (COVID-19). *JAMA Netw. Open* **3**, e2011834.
4. Guasp, M., C. Laredo and X. Urra (2020) Higher solar irradiance is associated with a lower incidence of COVID-19. *Clin. Infect. Dis.* in press. <https://doi.org/10.1093/cid/ciaa575>
5. Sagripanti, J. L. and C. D. Lytle (2007) Inactivation of influenza virus by solar radiation. *Photochem. Photobiol.* **83**, 1278–1282.
6. Madronich, S., L. O. Björn and R. L. McKenzie (2018) Solar UV radiation and microbial life in the atmosphere. *Photochem. Photobiol. Sci.* **17**, 1918–1931.
7. Sutton, D., E. W. Aldous, C. J. Warren, C. M. Fuller, D. J. Alexander and I. H. Brown (2013) Inactivation of the infectivity of two highly pathogenic avian influenza viruses and a virulent Newcastle disease virus by ultraviolet radiation. *Avian Pathol.* **42**, 566–568.
8. Lytle, C. D. and J. L. Sagripanti (2005) Predicted inactivation of viruses of relevance to biodefense by solar radiation. *J. Virol.* **79**, 14244–14252.
9. Wigginton, K. R., B. M. Pecson, T. Sigstam, F. Bosshard and T. Kohn (2012) Virus inactivation mechanisms: impact of disinfectants on virus function and structural integrity. *Environ. Sci. Technol.* **46**, 12069–12078.
10. Beck, S. E., R. A. Rodriguez, M. A. Hawkins, T. M. Hargy, T. C. Larason and K. G. Linden (2016) Comparison of UV-induced inactivation and RNA damage in MS2 phage across the germicidal UV spectrum. *Appl. Environ. Microbiol.* **82**, 1468–1474.
11. Sagripanti, J. and C. D. Lytle (2020) Estimated inactivation of coronaviruses by solar radiation with special reference to COVID-19. *Photochem. Photobiol.* **96**, 731–737.
12. Weiss, M. and M. C. Horzinek (1986) Resistance of Berne virus to physical and chemical treatment. *Vet. Microbiol.* **11**, 41–49.
13. Walker, C. M. and G. Ko (2007) Effect of ultraviolet germicidal irradiation on viral aerosols. *Environ. Sci. Technol.* **41**, 5460–5465.
14. Kowalski, W. (2009) *Ultraviolet Germicidal Irradiation Handbook. UVGI for Air and Surface Disinfection*, Springer, New York.
15. Schuit, M., S. Ratnesar-Shumate, J. Yoltiz, G. Williams, W. Weaver, B. Green, D. Miller, M. Krause, K. Beck, S. Wood, B. Holland, J. Bohannon, D. Freeburger, I. Hooper, J. Biryukov, L. A. Altamura, V. Wahl, M. Hevey and P. Dabisch (2020) Airborne SARS-CoV-2 is rapidly inactivated by simulated sunlight. *J. Infect. Dis.* **222**(4), 564–571.
16. Ratnesar-Shumate, S., G. Williams, B. Green, M. Krause, B. Holland, S. Wood, J. Bohannon, J. Boydston, D. Freeburger, I. Hooper, K. Beck, J. Yeager, L. A. Altamura, J. Biryukov, J. Yoltiz, M. Schuit, V. Wahl, M. Hevey and P. Dabisch (2020) Simulated sunlight rapidly inactivates SARS-CoV-2 on surfaces. *J. Infect. Dis.* **222**, 52281.
17. National Center for Atmospheric Research. (2020) Tropospheric ultraviolet and visible (TUV) radiation model. Available at: <https://www2.aocom.ucar.edu/modeling/tropospheric-ultraviolet-and-visible-tuv-radiation-model>. Accessed on 7 April 2020.
18. van Weele, M., R. J. van der, J. V. Geffen and R. Roebeling (2005) Space-based surface UV monitoring for Europe using SCIAMACHY and MSG. *Remote Sens. Clouds Atmos. X* **5979**, 59791K.
19. van Weele, M. and D. Bilt (2008) Surface solar and UV products for Europe by combination of MSG and SCIAMACHY (SUPREMACY). Final report. (53411).
20. O'Sullivan, F., E. Laird, D. Kelly, J. van Geffen, M. van Weele, H. McNulty, L. Hoey, M. Healy, K. McCarroll, C. Cunningham, M. Casey, M. Ward, J. Strain, A. M. Molloy and L. Zgaga (2017) Ambient UVB dose and sun enjoyment are important predictors of vitamin D status in an older population. *J. Nutr.* **147**, 858–868.
21. O'Sullivan, F., J. van Geffen, M. van Weele and L. Zgaga (2018) Annual ambient UVB at wavelengths that induce vitamin D Synthesis is associated with reduced esophageal and gastric cancer risk: a nested case-control study. *Photochem. Photobiol.* **94**, 797–806.
22. Van Geffen, J., M. Van Weele, M. Allaart and R. van der A (2017) TEMIS UV index and UV dose MSR-2 data products, version 2. Dataset. Royal Netherlands Meteorological Institute (KNMI). <https://doi.org/10.21944/temis-uv-msr2-v2>. Accessed on 06 May 2020.
23. Sliney, D. H. (2007) Radiometric quantities and units used in photobiology and photochemistry: recommendations of the Commission Internationale de L'Eclairage (International Commission on Illumination). *Photochem Photobiol.* **83**, 425–432.
24. Setlow, R. B. (1974) The wavelengths in sunlight effective in producing skin cancer: a theoretical analysis. *Proc. Nat. Acad. Sci* **71**, 3363–3366.
25. Otter, J. A., C. Donskey, S. Yezli, S. Douthwaite, S. D. Goldenberg and D. J. Weber (2016) Transmission of SARS and MERS coronaviruses and influenza virus in healthcare settings: the possible role of dry surface contamination. *J. Hosp. Infect.* **92**, 235–250.

26. Ianevski, A., E. Zusinaite, N. Shtaida, H. Kallio-Kokko, M. Valkonen, A. Kantele, K. Telling, I. Lutsar, P. Letjuka, N. Metelitsa, V. Oksenysh, U. Dumpis, A. Vitkauskienė, K. Stašaitis, C. Öhrmalm, K. Bondeson, A. Bergqvist, R. J. Cox, T. Tenson, A. Merits and D. E. Kainov (2019) Low Temperature And Low UV indexes correlated with peaks of influenza virus activity in northern europe during 2010-2018. *Viruses* **11**, 207.
27. Duan, S. M., X. S. Zhao, R. F. Wen, J. J. Huang, G. H. Pi, S. X. Zhang, J. Han, S. L. Bi, L. Ruan and X. P. Dong (2003) Stability of SARS coronavirus in human specimens and environment and its sensitivity to heating and UV irradiation. *Biomed. Environ. Sci.* **16**, 246–255.
28. Ren, S. Y., W. B. Wang, Y. G. Hao, H. R. Zhang, Z. C. Wang, Y. L. Chen and R. D. Gao (2020) Stability and infectivity of coronaviruses in inanimate environments. *World J. Clin. Cases* **8**, 1391–1399.
29. Eslami, H. and M. Jalili (2020) The role of environmental factors to transmission of SARS-CoV-2 (COVID-19). *AMB Express* **10**, 92.
30. Doremalen, N., D. H. van Morris, M. G. Holbrook, A. Gamble, B. N. Williamson, A. Tamin, J. L. Harcourt, N. J. Thornburg, S. I. Gerber, J. O. Lloyd-Smith, E. de Wit and V. J. Munster (2020) Aerosol and surface stability of SARS-CoV-2 as compared with SARS-CoV-1. *N. Engl. J. Med.* **382**, 1564–1567.
31. Kampf, G., D. Todt, S. Pfaender and E. Steinmann (2020) Persistence of coronaviruses on inanimate surfaces and their inactivation with biocidal agents. *J. Hosp. Infect.* **104**, 246–251.
32. ECDC (2020) Coronavirus disease 2019 (COVID-19) in the EU / EEA and the UK – tenth update, 10th August 2020. Eur. Cent. Dis. Prev. Contro, (August).